SciMedCentral

Annals of Vascular Medicine & Research

Research Article

CFD-Based Virtual Comparative Analysis of Treatment Efficacy for a Blunt Thoracic Aortic Injuries Case

Ali Hakimi[1], Amir Alimohammadi[1], M. Soltani[1-5], Hamidreza Pouraliakbar[6], Parham Sadeghipour[6], and Mona Alimohammadi[1]*

[1]*Department of Mechanical Engineering, K. N. Toosi University of Technology, Iran*
[2]*Department of Integrative Oncology, BC Cancer Research Institute, Canada*
[3]*Department of Electrical and Computer Engineering, University of Waterloo, Canada*
[4]*Centre for Sustainable Business, International Business University, Canada*
[5]*Balsillie School Fellow at the Balsillie School of International Affairs (BSIA), Canada*
[6]*Vascular Disease and Thrombosis Research Center, Rajaie Cardiovascular Medical and Research Institute, Iran*

***Corresponding author**
Mona Alimohammadi, Department of Mechanical Engineering, K. N. Toosi University of Technology, Iran, Tel No: +989915112261

Submitted: 05 December 2025
Accepted: 05 March 2026
Published: 06 March 2026
ISSN: 2378-9344

Copyright
© 2026 Hakimi A, et al.

OPEN ACCESS

Keywords
- Computational Fluid Dynamics
- Blunt Thoracic Aortic Injury
- Beta-Blocker
- Medical Treatment
- Thoracic Endovascular Aortic Repair
- Virtual Endovascular Planning
- Hemodynamic Analysis

Abstract

The clinical treatment outcomes of blunt thoracic aortic injury, the second leading cause of death in traumatic incidents, remain ambiguous even with significant advances in imaging techniques. One of the novel non-invasive investigations utilises computational fluid dynamics, which can proficiently predict therapeutic risk probabilities, proving beneficial for clinical applications. This study represents a virtual therapeutic investigation, assessing non-invasive and invasive treatment methods on the specific patient with its virtual revised cases. Pressure, flow velocity, and wall shear stress indices under the two-element Windkessel model boundary conditions were calculated in the patient's aorta for three therapeutic applications. Furthermore, to scrutinize therapeutic effects on different aortic locations, the patient's vessel was examined in segments, and the numerical variations of indices were graphically represented. Results indicate that using beta-blockers as a non-invasive treatment can control pressure adequately, delay the need for invasive treatments, and reduce the risk of aortic damage. In contrast, the virtual surgical procedure as an invasive treatment displayed increased pressure and wall stress on the aorta, making potentially vulnerable areas more prominent. However, the complex flow pattern was reduced with anatomical correction. A virtual study of pharmacological treatment (beta-blocker) post-surgery was also conducted; the pressure reduction by the beta-blocker neutralised the increased wall stress from surgery and controlled the risk in concerning areas. Analysing and comparing the results using the methodologies employed in this study can provide valuable clinical insights into selecting therapeutic approaches for blunt thoracic aortic injuries.

INTRODUCTION

Blunt thoracic aortic injury (BTAI) is one of the acute cardiovascular emergencies often caused by traumatic incidents, predominantly vehicular accidents (50%) and pedestrian-vehicle collisions (37%) [1,2]. Among patients with blunt trauma, thoracic aortic injury (TAI) is the second leading cause of death after head injuries [2-4]. Complications such as hemorrhage, cardiac tamponade, ischemia, and delayed rupture can be initially acute and become fatal if not immediately addressed [5-7]. Rapid deceleration forces result in shear stresses on the aorta, inducing morphological alterations [8-10]. One of the primary clinical criteria for assessing trauma-induced aortic risk is the measurement of pseudoaneurysm size and its categorisation based on injury extent [9]. The appropriate BTAI therapeutic approach is contingent on size, patient's health status, and aneurysm location [10]. In essence, the therapeutic scenario is individually tailored based on the risk-benefit analysis for each specific patient [10]. Patients with minimal injury don't require endovascular intervention; anti-hypertensive treatment with beta-blockers can limit further progression [2-8]. Those with moderate injuries can undergo semi-invasive such as Thoracic endovascular aortic repair (TEVAR) procedures once other injuries have stabilised, while patients with severe injuries require immediate repair using invasive surgical interventions [2-12]. Current

clinical decisions are majorly based on medical imaging; notwithstanding advancements in imaging techniques, there is still ambiguity concerning a consistent therapeutic approach [13,14]. Computational modeling and structural hemodynamic simulations can provide risk determination with an array of indices beyond size [15,16]. According to research, employing CFD simulation combined with the finite element method (FEM) can provide valuable hemodynamic indices [17-21]. In this study, hemodynamic indices under three therapeutic scenarios were obtained using a two-parameter Windkessel CFD simulation for a patient-specific case. Initially, the patient's baseline hemodynamic status was evaluated, and subsequently, the impact of each therapeutic scenario on the hemodynamics was assessed. For non-invasive therapy scenarios, the pharmacological effect of using beta-blockers (BB) was analysed [2]; this method reduces left ventricular contraction by modulating ion levels [17-24], and diminishes cardiac output, resulting in a heart rate reduction [20-25]. This treatment reduces wall stress, decreases blood pressure, and subsequently slows aneurysm growth, potentially preventing ruptures, and further dissections, and obviating the need for imminent surgical interventions [26-28]. For invasive therapy scenarios, a virtual surgical intervention was examined on the studied patient [2-29]. This technique, involving complete aneurysm removal followed by tissue grafting to the aortic wall, is employed due to its high invasive risk [29-33], especially in specific situations where endovascular repair isn't suitable or feasible [32]. An essential aspect of medical management is post-surgical pharmacotherapy, which can also mitigate injuries stemming from surgical interventions [34]. This study has delved into the impact of post-surgical pharmacological treatment to comprehend its influence on the patient's hemodynamic parameters.

In this study, we utilised the pressure gradient and Wall Shear Stress (WSS) as hemodynamic indicators, which proficiently delineate the pressure condition on the aortic wall [35]. For a meticulous analysis of various aortic segments, we have segmented the aorta into five distinct sections. Although past research has explored therapeutic effects on aortic diseases [17-37], a quantitative evaluation of these indicators in each separate section and the distinct impact of the aforementioned therapeutic methods on each segment is an innovative approach. Ultimately, this investigation aims to assist clinical researchers in implementing the most effective therapeutic scenario when confronted with BTAI conditions.

METHODOLOGY

A three-dimensional (3D) fluid domain was generated from a collection of 780 Digital Imaging and Communications in Medicine (DICOM) images of a 59-year-old male patient who had sustained trauma from an accident, resulting in the formation of a pseudoaneurysm in the aortic arch region. The fluid domain was extracted using MIMICS Research 21.0 (2018 version, Materialise, Leuven, Belgium). The resolution of the computed tomography angiography (CTA) images was 0.95 mm per pixel, the diameter of the ascending aorta (D) was approximately 3 cm, and the diameter of the aorta at the aneurysm site prior to intervention was about 4.7 cm. Processes such as thresholding, crop mask, split mask, and others were employed to adequately construct the geometry.

The right innominate artery (including right subclavian artery (RS), right common carotid artery (RCC)), left carotid common artery (LCC), and left subclavian artery (LS) were retained on the aortic arch. However, the extraction of the iliac arteries and smaller vascular branches were omitted due to the low quality of the images. Ultimately, the boundaries were trimmed with horizontal parallel planes to ensure the inlets and outlets were aligned along a single axis. For the virtual surgery, utilising the MIMICS software based on the aorta's cross-sectional area before and after the aneurysm and under the supervision of a vascular surgeon, the aortic morphology was adjusted. Due to the aneurysm's expansion up to the LS artery, the decision was made to remove this branch during the virtual surgery, reducing the aorta's diameter at the aneurysm site post-surgery to 3.7 cm. In Figure 1, a cross-sectional view of the reconstructed 3D geometries is mapped alongside the CT images for a better understanding of the patient-specific domain at multiple scales.

The fluid domain was meshed using ANSYS Meshing 18.2 (ANSYS Inc., Canonsburg, PA, USA). This geometry consists of approximately 185,500 and 71,000 tetrahedral cells and node numbers in its initial state and about 196,000 and 72,000 tetrahedral cells and node numbers post-virtual surgery. To minimize computational errors, seven prism layers with a growth rate of 1.2 were applied near the wall for both geometries. To ensure element compatibility in analyzing the two existing fluid domains, meshing was performed with identical volumetric properties. Mesh independence of the fluid domain was evaluated to examine the maximum percentage difference between the grids and thus to save on computational costs, the medium mesh was selected.

The continuity and Navier-Stokes equations (Eq. (1),(2)) were solved using the CFX 2019 R3 software (ANSYS Inc., Canonsburg, PA, USA) based on the finite volume method. For post-processing of data, ANSYS CFD-Post software

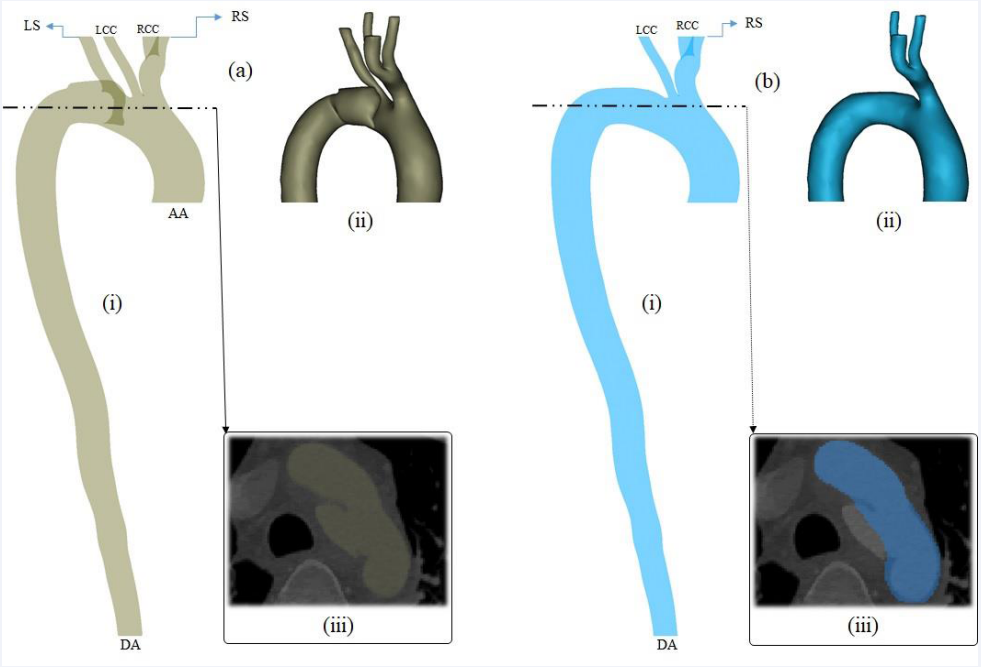

Figure 1 a. (i) Patient-specific fluid domain, (ii) 3D geometry at the aneurysm location, and (iii) cross-sectional view of the aneurysm site in the aortic arch prior to virtual surgery. b. (i) Patient-specific fluid domain, (ii) 3D geometry at the aneurysm location, and (iii) cross-sectional view of the aneurysm site in the aortic arch post-virtual surgery.

was employed. The discretization of governing equations involves a second-order backward Euler scheme with a time step of 0.01 seconds, and the maximum mean squared residual errors have been set to 1×10^-5.

$$\nabla \cdot \vec{u} = 0 \tag{1}$$

$$\rho \frac{\partial \vec{u}}{\partial t} + \rho(\vec{u} \times \nabla)\vec{u} + \nabla p - \mu \Delta \vec{u} = 0 \tag{2}$$

Boundary Conditions

Blood was considered an incompressible fluid with a density of 1056 kg/m^3 with non-Newtonian properties. Its viscosity is determined by the Carreau-Yasuda viscosity model (Eq.(3)) [36], in which μ is the viscosity, γ' is the shear rate, μ_0 is the Carreau-Yasuda zero shear viscosity, and μ_∞, a, m, and λ_{CY} are respectively the Carreau-Yasuda infinite shear viscosity, Yasuda power-law exponent, Carreau-Yasuda power-law index, and Carreau-Yasuda time constant [38].

$$\mu = (\mu_0 - \mu_\infty)(1 + (\lambda_{CY}\gamma')^a)^{(m-1)/a} + \mu_\infty \tag{3}$$

To aid in direct comparison between various cases, the vessel wall has been assumed to be rigid. Additionally, due to the high computational cost and the alteration in vessel properties following invasive interventions, the use of Fluid-Structure Interaction (FSI) was deemed outside the scope of this study. Blood first enters the fluid domain from the AA and then, upon reaching the aortic arch region, it branches off into the RS, RCC, LCC, and LS before eventually moving towards the distal abdominal (DA) region. Due to the unavailability of the patient's echocardiography data, the velocity profile of the AA was estimated based on an idealised semi-sinusoidal signal (Eq.(4)) [39], where V_0 is the peak blood velocity at the inlet, T_{ej} is the systolic ejection time, and T is the cardiac cycle length.

$$V(t) = \begin{cases} V_0 \sin\left(\frac{\pi t}{T_{ej} T}\right) & if\ 0 < t < T_{ej} T \\ 0 & if T_{ej} T \le t < T \end{cases} \tag{4}$$

The values for V_0, T_{ej}, and T were taken to be 96.1 cm/s, 0.273 seconds, and 0.731 seconds, respectively [18].

For the outlets, a Windkessel model of the 2-element type (WK2) was utilized (Eq. (5)), which serves as a realistic dynamic boundary condition to represent the effect of distal vessels on the outlets. The WK2 is a hydraulic-electric analogy (0-D) in which, based on the governing equation, the blood flow (Q) and blood pressure (P) are analogous to electrical current and voltage, respectively. Moreover, the energy storage property of blood in the vessel was simulated with a capacitor (C), and the resistance of the vessel against flow was likened to electrical resistance (R) [40].

$$P = RQ - RC\frac{dP}{dt} \tag{5}$$

To obtain the WK2 parameters, available data from an actual patient case was personalized for the patient under study [36]. The final values for *R* and *C* are presented in Table 1

For therapeutic application design for the patient, both non-invasive and invasive approaches were investigated. In the non-invasive approach, pharmacotherapy using BB was examined [41,42]. To assess the maximum effect of virtual pharmacotherapy using BB with the aim of controlling blood pressure within the normal heart rate range down to about 55 BPM, BB physiologically responds to the released ions in the left ventricle, reducing its contraction. This mechanism leads to a reduced heart rate, subsequently lowering blood pressure [20-24]. In this study, the effect of BB is considered solely to alter the cardiac output, and the peripheral vessel resistance is not affected by the drug [43].

Virtual surgery, aiming to predict hemodynamic flow patterns resulting from morphological patterns, was evaluated as one of the invasive therapeutic methods [44]. This invasive method is applied to prevent rupture and aneurysm dissection due to excessive wall thinning [45,46]. This intervention involves repairing or replacing the weakened or damaged portion of the aorta with a synthetic graft [47,48]. This method, involving aorta reconstruction and repair, was performed to revert its state pre-damage. Due to the presence of an aneurysm in the aortic arch and the involvement of the LS branch, the decision was made to remove this artery. The resistance value in the other outlet branches, given the unchanged anatomy, was considered the same as pre-surgery. Moreover, to maintain consistency, an inlet velocity profile was used for both ascending aorta speeds before and after the procedure [18-49]. Also, for combined therapy assessment, the effect of BB on the corrected post-surgical fluid domain was studied to control pressure in the normal range while preventing rupture and initiating dissection [37-51].

In the current study, an analysis of the impact of various therapeutic methods on hemodynamic criteria was conducted. The spatial distribution of pressure on the patient's aorta wall, the spatial flow streamlines distribution; the time-averaged wall shear stress (TAWSS), the oscillatory shear index (OSI), Highly Oscillatory and Low Magnitude Shear (HOLMES), and the relative residence time (RRT) were considered as visual hemodynamic indices in the patient and the three virtual treatment study cases. Additionally, the percentage difference in pressure, flow velocity, and TAWSS, as the primary criteria among the mentioned cases, was charted.

Table 1: Final tuned Wk2 parameter

	RS	RCC	LCC	LS	DA
R (mmHg)	3.83	4.08	6.83	4.45	1.79
C (ml/mmHg)	0.31	0.29	0.18	0.27	0.67

RESULTS

The indices investigated in this study pertain to WSS analysis, a crucial aspect of hemodynamics in the cardiovascular system. The studied indices encompass TAWSS, OSI, HOLMES, and RRT. Each of these metrics plays a significant role in elucidating the complex flow patterns and biomechanical forces experienced by the blood vessels within the cardiovascular system.

TAWSS

TAWSS is an important WSS indicator which is prescribed by Eq.(6) :

$$TAWSS = \frac{1}{T}\int_0^T \left|\vec{\tau}\ (t)\right| dt \tag{6}$$

where $\vec{\tau}(t)$ and T are WSS vectors at time t and the total time of the cardiac cycle. Figure 2a presents the spatial distribution of TAWSS within the aorta. In general, higher TAWSS values are observed in the upper branches of the aorta, including RS, RCC, LCC, and LS branches. Under drug treatment employing BB, a slight decrease in TAWSS is evident in the aorta. Conversely, following the application of VS, an increase in TAWSS is observed throughout the aorta, except at the location of the aneurysm where a reduction in this index is evident. Strikingly, when both treatment methods are concurrently employed, a general reduction in TAWSS is observed throughout the aorta, with notable effects in the branches of the vessel.

Furthermore, as depicted in Figure 2b, the graph illustrates the percentage changes in the maximum TAWSS in different sections of the patient's aorta. Yielded a remarkable increase in the maximum TAWSS index value across all sections, except V1. Especially significant changes induced by the VS treatment were prominently observed in the V1 and V5 sections. Conversely, the administration of drug treatment intervention led to a significant reduction in the magnitude of TAWSS within all aortic segments.

OSI

Oscillatory shear index (OSI) is another meaningful WSS indicator and can be achieved from the following equation:

$$OSI = 0.5\left(1 - \frac{\left|\frac{1}{T}\int_0^T \vec{\tau}(t)\right|}{TAWSS}\right) \tag{7}$$

With values ranging from 0 to 0.5, this parameter

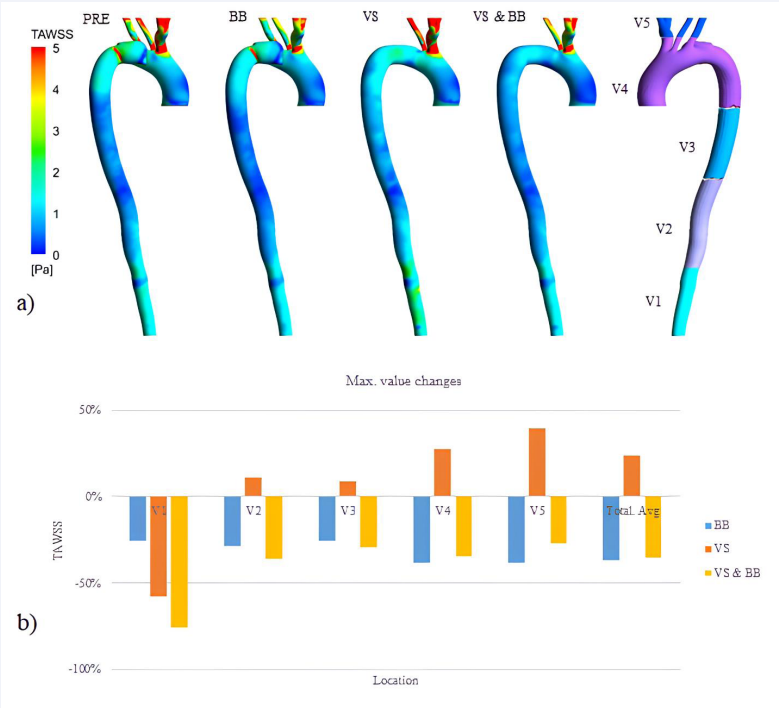

Figure 2 a) The spatial distribution of TAWSS for all four investigated modes (PRE, BB, VS, BB & VS). b) The percentage changes in the maximum TAWSS in different sections of the patient's aorta.

quantifies the variations in forces acting on the endothelium cells [36]. While larger values show a more irregular direction of WSS forces, an OSI value of zero suggests unidirectional wall shear forces.

Figure 3 illustrates the spatial distribution of OSI. Evidently, high OSI values are concentrated in the Arch region of the aorta. Under drug treatment with BB, the OSI values display an increase in the arch. Similarly, following VS intervention, OSI values show an increase in both the arch and certain areas of the DA.

Significantly, the interaction between both treatment modalities results in a consistent increase in OSI values in the arch region, while the DA area experiences a decrease in OSI.

HOLMES

To further elucidate the interplay between the two parameters, TAWSS and OSI, we scrutinize the HOLMES index. This metric offers a potent instrument for forecasting plaque localization and subsequent progression:

$$HOLMES = TAWSS(0.5 - OSI) \tag{8}$$

Figure 4 presents the spatial distribution of the HOLMES under three distinct treatment modes. Remarkably, high HOLMES values are prominently observed in the upper branches of the aorta. Upon therapeutic intervention utilizing BB, a notable reduction in HOLMES values is observed across the aorta. Conversely, following the application of VS, HOLMES values decrease at the location of the aneurysm but display an increase in other areas of the aorta.

Noteworthy is the investigation of the simultaneous effect of both treatments, which reveals a general decrease in HOLMES values across the aorta.

RRT

The relative residence time (RRT) is calculated as:

$$RRT = \frac{1}{TAWSS(1-2\cdot OSI)} \tag{9}$$

RRT calculates the duration of residence of particles close to the wall, and it is a single measure of oscillating and low-shear stress

Figure 5 displays the spatial distribution of the RRT index. Particularly, the highest RRT values are observed in the AA and the arch region. Following drug treatment, a general increase in RRT is evident across the aorta. Conversely, after the application of VS, specific changes in RRT are not prominently observed, but the location of the maximum RRT value has shifted within the arch region.

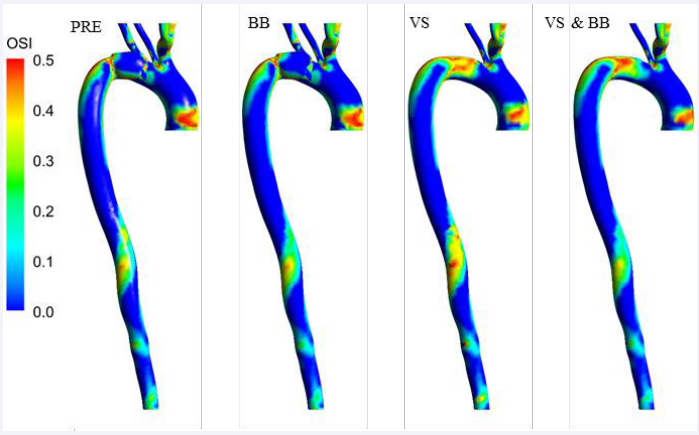

Figure 3 The spatial distribution of OSI for all four investigated modes (PRE, BB, VS, BB & VS)

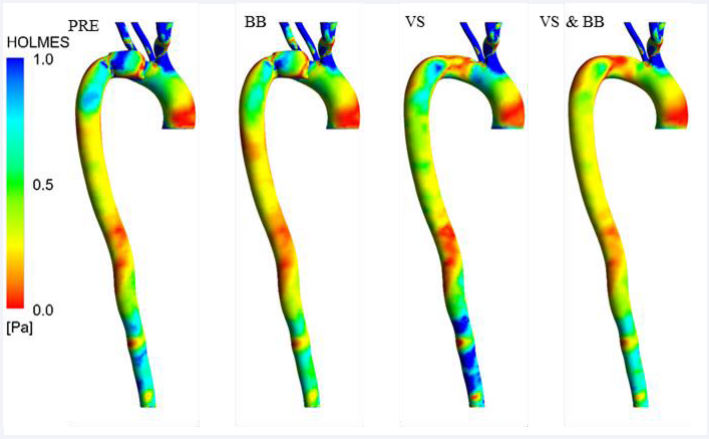

Figure 4 The spatial distribution of the HOLMES for all four investigated modes (PRE, BB, VS, BB & VS)

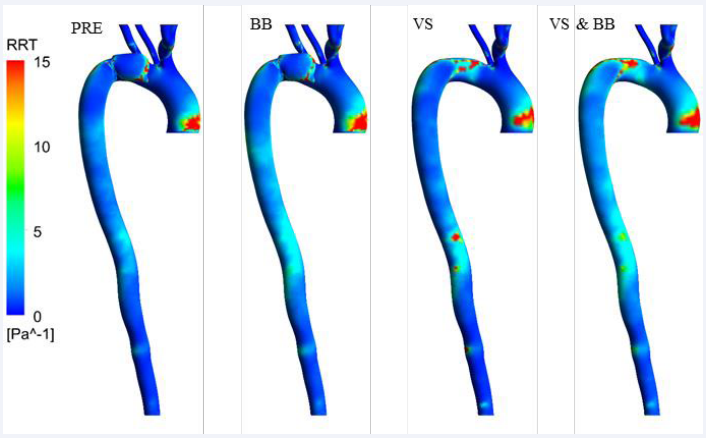

Figure 5 The spatial distribution of the RRT for all four investigated modes (PRE, BB, VS, BB & VS)

Of particular interest is the combined effect of both treatment modalities in the simulation, where RRT shows a general increase throughout the aorta. However, in certain locations of aortic torsion within the DA area, negligible reductions in RRT values are noted.

Pressure

Figure 6a. presents the pressure spatial distribution during systole under three different treatment conditions. Following drug intervention, a prominent decrease in systolic pressure is observed along the aorta. Additionally, the pressure difference between the AA and DA is reduced during systole. During diastole, the pressure difference between AA and DA, with the exception of the upper branches, is also reduced. Importantly, the maximum pressure during the cardiac cycle occurs in the descending aorta. Conversely, under VS intervention, the systolic pressure shows an overall increase throughout the aorta, except in the DA where the pressure decrease is insignificant. Moreover, the pressure gradient attains its highest value among all three treatment methods. During diastole, pressure exhibits a decrease throughout the aorta, except in the DA.

Astonishingly, the simultaneous application of both treatment methods results in a pronounced decrease in both systolic and diastolic pressure values. Throughout the cardiac cycle, the maximum pressure occurs in the descending aorta, indicating the influence of these treatment modalities on pressure dynamics in this region.

In Figure 6b, the graphical representation of maximum pressure changes during systole is provided. After performing VS, resulted in a significant reduction of maximum pressure solely in the V1 section, with the most pronounced effect observed in the V4 section. On the other hand, drug treatment intervention led to a notable decrease in maximum pressure across all segments of the vessel; Particularly noteworthy is the combined application of both treatment methods, which exhibited the most substantial effect in reducing maximum pressure.

In contrast, Figure 6c, displaying the minimum pressure changes, reveals that therapeutic interventions do not follow a uniform trend across different segments of the vessel. Notably, in the V5 section, minimal pressure changes were observed only with the utilisation of VS.

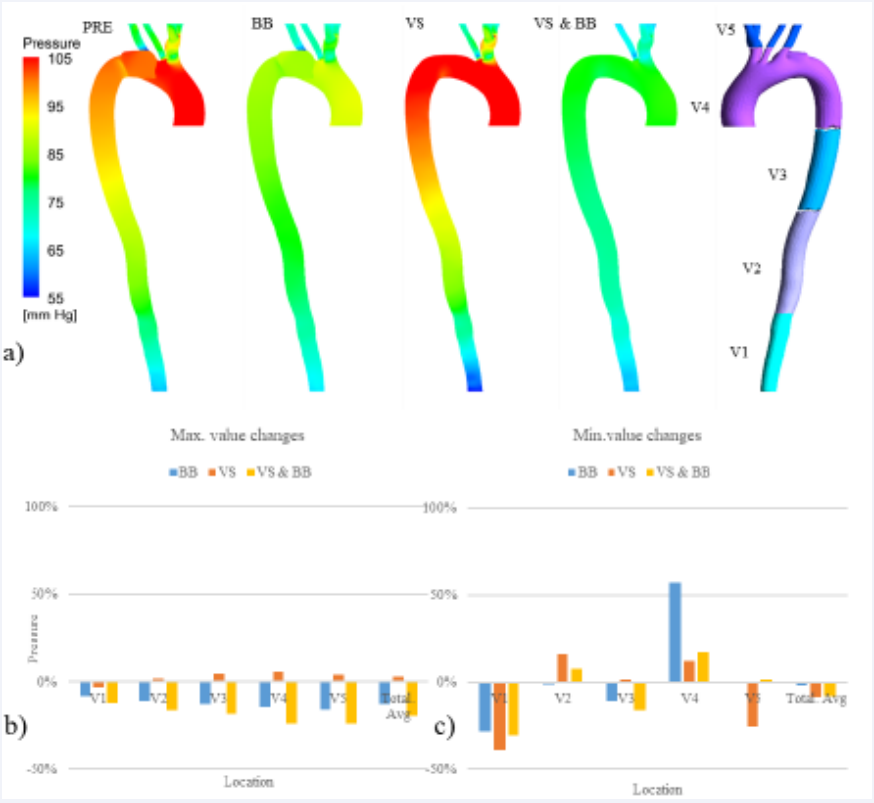

Figure 6 a) Pressure distribution for all four investigated modes (PRE, BB, VS, BB & VS) during systolic blood pressure. b) The graphical representation of maximum pressure changes during systole. c) the graphical representation of minimum pressure changes during systole

Velocity

Figure 7a presents the velocity spatial distribution visualization. In the pre-surgical mode in the thoracic aorta, vortex flow is caused by pseudoaneurysm. The application of drug treatment in this patient has resulted in a notable reduction in velocity values, particularly evident in the upper branches of the aorta. Furthermore, during diastole, there is a pronounced increase in the rate of rotation of flow lines, accompanied by a decrease in outflow from the upper.

On the other hand, therapeutic intervention using VS has led to an increase in flow velocity during systole in the upper branches and DA. During diastole, the flow velocity in the arch has decreased, accompanied by a reduction in the rotation of flow lines in these regions, while the outflow of flow lines from the branches has increased. Impressively, when both treatments are applied concurrently, the velocity during systole experiences a decrease, and a conspicuous increase in the rotation of flow lines becomes apparent.

Figure 7b illustrates the graphical representation of maximum velocity changes during systole is provided. The application of surgical intervention resulted in an increase in velocity within the aortic sections; however, this observed increase was found to be statistically insignificant in the V4 section. On the other hand, drug intervention utilizing BB led to a notable reduction in maximum velocity across different aortic segments, both pre- and post-surgery. Remarkably, the effect of BB demonstrated a higher consistency in the pre-surgical mode compared to the post-surgical mode.

DISCUSSION AND CONCLUSION

In the current study, three-dimensional flow simulations were performed on a patient with a BTAI, delving into various hemodynamic indices. The principal objective of this research was to investigate and contrast different therapeutic approaches.

The results presented in Figure 6 indicate that the patient suffers from a sudden decrease in aortic pressure. Additionally, the aortic pressure displays an uneven distribution. Elevated pressure in the AA segment and its abrupt fluctuations heighten the probability of complications such as aortic dilation, Hemodynamic Instability, and aneurysm expansion [52-54]. Vascular

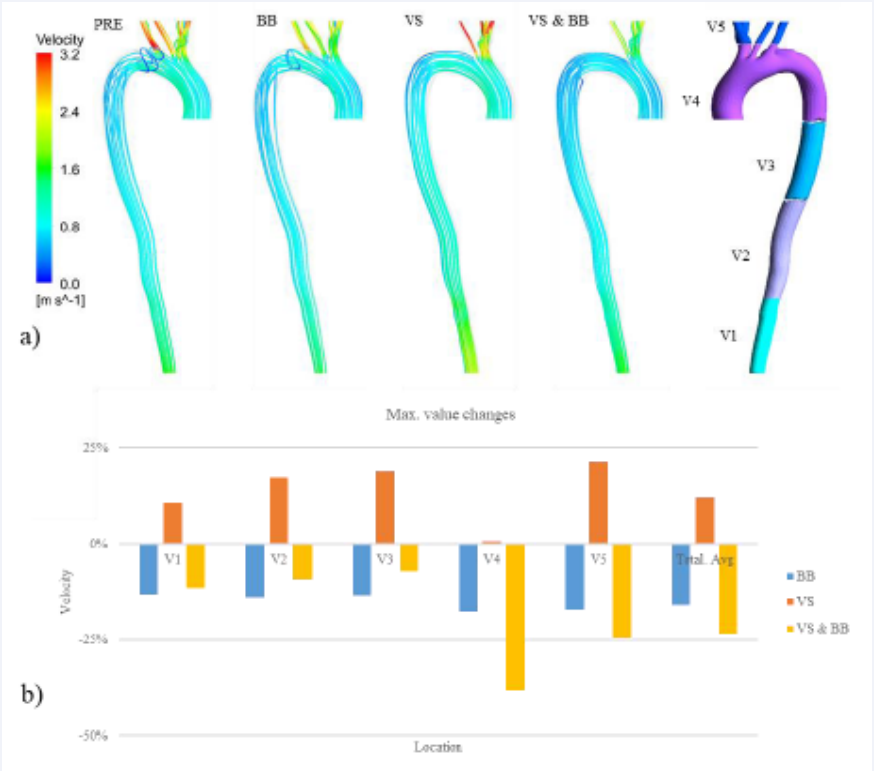

Figure 7 a) Velocity spatial distribution for all four investigated modes (PRE, BB, VS, BB & VS) during systole. b) The graphical representation of maximum velocity changes during systole

stiffness, a pivotal factor in cardiovascular diseases, can be attributed to elevated blood pressure [55]. Given the patient's uneven blood pressure distribution, the existing hypertension could be the cause of arterial wall stiffness, potentially leading to downstream organ failure [56].

Pharmacological interventions lead to a reduction in pressure gradient, primarily due to the decrease in peak pressure. Such therapeutic approaches can prevent possible damages from elevated pressure [17]. However, After virtual surgery at the aneurysm site (VS), the patient's maximum pressure increases while maintaining the uneven pressure distribution, a phenomenon also observed in prior research [57-60]. It's worth noting that primary surgical interventions aim to prevent rupture, internal bleeding, and potential damage to the aortic arch, among others [61,62].

Upon simultaneous application of both therapeutic methods, there was a considerable decrease in peak pressure and the pressure distribution became considerably more uniform compared to the patient's initial state. According to the Figure 6a,b, the most significant impact on reducing the peak pressure across various aortic sections was observed with the concurrent application of both treatment methods.

Examining the patient's aorta in Figure 7 reveals observable vortex flow patterns at the thoracic aorta, one of the hemodynamics side-effects of pseudoaneurysm caused by this disease (BTAI) [63]. Moreover, increased flow velocity is evident in the upper branches of the aorta. The flow velocity demonstrates an inhomogeneous distribution, a phenomenon that can be attributed to the aorta's anatomical irregularities [64]. Elevated velocity and vortex presence at the aneurysm location enhance the likelihood of complications such as rupture, thrombosis, atherosclerosis, and dissection [65-68].

As observed, the peak velocity post-pharmacological treatment has considerably decreased across the vessel; the flow lines have become more uniform, and the vortex patterns at the aneurysm site have diminished [17]. However, After virtual surgery at the aneurysm site (VS), there's a noticeable velocity increase in all segments except at the aneurysm position; complex flow patterns in the aorta, especially at the aneurysm and aortic arch sites, have diminished [69,70]. In a similar study by Filipovic at el, a reduction in complex flow patterns following aortic repair is reported [59].

The evaluation of both therapeutic methods applied simultaneously led to a velocity decrease in the aorta, particularly in its upper branches, rendering the flow the most uniform among the three examined methodologies. These findings underscore the efficacy of BB in reducing velocity and the influence of VS in diminishing complex flow patterns during systole.

Based on the acquired results, the patient suffers from elevated wall shear stress (WSS) in the surrounding vessel walls of the upper branches, which can potentially induce damage to the endothelial lining of the aorta [71]. Additionally, the segment of the abdominal aorta displays a low shear index, where a time-averaged wall shear stress (TAWSS) between 0 and 1 can escalate the likelihood of atherosclerotic plaque formation [72]. Pharmacological intervention has effectively decreased this index throughout the aorta, particularly in the upper branches. Chen et al., in a 2021 study, explains that elevated TAWSS levels can cause endothelial cell destruction in the visceral arteries and aorta, resulting in intimal hyperplasia of the arterial wall and aggravating stenosis [73]; As a result, reducing the amount of TAWSS can lower the risk of the mentioned cases. After virtual surgery, the TAWSS has generally increased, decreasing the probability of atherosclerosis in the abdominal aorta region [73]. Implementing both therapeutic strategies normalizes the TAWSS values.

In the ascending and abdominal sections of the aorta, a high oscillatory shear index (OSI) is observed, which might promote the accumulation of low-density lipoprotein cholesterol (LDL) [74]. Different therapeutic methods don't produce significant alterations in this index. Elevated relative residence time (RRT) under such conditions also amplifies the likelihood of vascular inflammatory marker absorption, leading to aneurysm expansion [75].

The HOLMES index can proficiently predict regions susceptible to calcification, a primary precursor for atherosclerosis [76]. This index exhibits its minimal value in the ascending and abdominal aorta, indicating a predisposition to plaque formation. Pharmacological treatment, surgical intervention, and the simultaneous application of both methods result in a decrease, increase, and decrease in HOLMES, respectively. Given the negligible changes in OSI, the HOLMES variations are predominantly based on TAWSS.

In conclusion, the findings suggest that virtual pharmacotherapy significantly impacts the reduction of both maximum and pressure gradient, diminishing the risk of damage due to elevated pressures in the patient. Furthermore, it can be utilised to decrease wall stress in high-risk areas. However, it should be noted that higher dosages of BB may increase the propensity for plaque

formation, which requires medical oversight. On the other hand, virtual surgical intervention reduces the risk of rupture and complex flow patterns in the aorta, especially around the aneurysm location. Still, it does result in an increased pressure gradient, subsequently raising the speed and WSS, especially in the upper branches, warranting risk management considerations. Nevertheless, surgical intervention elevates the minimal HOLMES level, reducing areas prone to plaque formation. The concurrent application of both strategies simultaneously reduces the risk associated with elevated pressure and atherosclerotic plaque formation, potentially representing the optimal therapeutic approach to minimize damage risk. This research offers critical guidance to clinicians, assisting in choosing the most suitable therapeutic approach for this condition.

LIMITATIONS

Due to the unavailability of patient-specific inflow velocities, existing literature data were employed; however, future studies could incorporate patient-specific data for a more in-depth analysis. Advanced imaging techniques such as 4D MRI could be utilized to extract patient-specific ventricular output for more accurate evaluations [49]. To improve modeling and validation approaches, further studies involving a larger patient cohort are needed. Another limitation is the rigid wall approximation; while FSI analysis makes the simulation conditions more realistic, studies showed that FSI only differs the absolute value of indices and does not vary the locations of high and low values. Nonetheless, the primary focus of this study is to compare different therapeutic approaches for aortic aneurysms resulting from BTAI, and to examine their distinct impacts on different segments of the aorta. This is an aspect less commonly covered in existing literature.

DATA AVAILABILITY STATEMENT

"The raw data used in this research is unavailable for public access to protect the privacy of resources but data or any question regarding the study are available from the corresponding author on reasonable request."

REFERENCES

1. Teixeira PG, Inaba K, Barmparas G, Georgiou C, Toms C, Noguchi TT, et al. Blunt thoracic aortic injuries: an autopsy study. J Trauma. 2011; 70: 197-202.
2. Harris DG, Rabin J, Starnes BW, Khoynezhad A, Conway RG, Taylor BS, et al. Evolution of lesion-specific management of blunt thoracic aortic injury. J Vasc Surg. 2016; 64: 500-505.
3. Dosios TJ, Salemis N, Angouras D, Nonas E. Blunt and penetrating trauma of the thoracic aorta and aortic arch branches: an autopsy study. J Trauma. 2000; 49: 696-703.
4. Neschis DG, Scalea TM, Flinn WR, Griffith BP. Blunt aortic injury. N Engl J Med. 2008; 359: 1708-1716.
5. Richens D, Field M, Neale M, Oakley C. The mechanism of injury in blunt traumatic rupture of the aorta. Eur J Cardiothorac Surg. 2002; 21: 288-293.
6. Steenburg SD, Ravenel JG. Acute traumatic thoracic aortic injuries: experience with 64-MDCT. AJR Am J Roentgenol. 2008; 191: 1564-1569.
7. Fox N, Schwartz D, Salazar JH, Haut ER, Dahm P, Black JH, et al. Evaluation and management of blunt traumatic aortic injury: a practice management guideline from the Eastern Association for the Surgery of Trauma. J Trauma Acute Care Surg. 2015; 78: 136-146.
8. Fabian TC, Davis KA, Gavant ML, Croce MA, Melton SM, Patton JH Jr, et al. Prospective study of blunt aortic injury: helical CT is diagnostic and antihypertensive therapy reduces rupture. Ann Surg. 1998; 227: 666-676.
9. Fortuna GR Jr, Perlick A, DuBose JJ, Leake SS, Charlton-Ouw KM, Miller CC 3rd, et al. Injury grade is a predictor of aortic-related death among patients with blunt thoracic aortic injury. J Vasc Surg. 2016; 63: 1225-1231.
10. Quiroga E, Starnes BW, Tran NT, Singh N. Implementation and results of a practical grading system for blunt thoracic aortic injury. J Vasc Surg. 2019; 70: 1082-1088.
11. Joseph M. Galante, Raul Coimbra. Thoracic Surgery for the Acute Care Surgeon. Cham: Springer International Publishing. 2021.
12. Isselbacher EM, Preventza O, Hamilton Black J 3rd, Augoustides JG, Beck AW, Bolen MA, et al. 2022 ACC/AHA Guideline for the Diagnosis and Management of Aortic Disease: A Report of the American Heart Association/American College of Cardiology Joint Committee on Clinical Practice Guidelines. Circulation. 2022; 146: e334-e482.
13. Ledesma M, Alva C, Gómez FD, Sánchez-Soberanis A, Díaz y Díaz E, Benítez-Pérez C, et al. Results of stenting for aortic coarctation. Am J Cardiol. 2001; 88: 460-462.
14. Rafiei D, Abazari MA, Soltani M, Alimohammadi M. The effect of coarctation degrees on wall shear stress indices. Sci Rep. 2021; 11: 12757.
15. Mendez V, Di Giuseppe M, Pasta S. Comparison of hemodynamic and structural indices of ascending thoracic aortic aneurysm as predicted by 2-way FSI, CFD rigid wall simulation and patient-specific displacement-based FEA. Comput Biol Med. 2018; 100: 221-229.
16. Nathan DP, Xu C, Gorman JH 3rd, Fairman RM, Bavaria JE, Gorman RC, et al. Pathogenesis of acute aortic dissection: a finite element stress analysis. Ann Thorac Surg. 2011; 91: 458-463.
17. Abazari MA, Rafiei D, Soltani M, Alimohammadi M. The effect of beta-blockers on hemodynamic parameters in patient-specific blood flow simulations of type-B aortic dissection: a virtual study. Sci Rep. 2021; 11: 16058.
18. Dadras R, Jabbari A, Asl NK, Soltani M, Rafiee F, Parsaee M, et al. In-silico investigations of haemodynamic parameters for a blunt thoracic aortic injury case. Sci Rep. 2023; 13: 8355.
19. Keshavarz-Motamed Z, Rikhtegar Nezami F, Partida RA, Nakamura K, Staziaki PV, Ben-Assa E, et al. Elimination of Transcoarctation Pressure Gradients Has No Impact on Left Ventricular Function or Aortic Shear Stress After Intervention in Patients With Mild Coarctation. JACC Cardiovasc Interv. 2016; 9: 1953-1965.

20. Lipp SN, Niedert EE, Cebull HL, Diorio TC, Ma JL, Rothenberger SM, et al. Computational Hemodynamic Modeling of Arterial Aneurysms: A Mini-Review. Front Physiol. 2020; 11: 454.

21. Romarowski RM, Lefieux A, Morganti S, Veneziani A, Auricchio F. Patient-specific CFD modelling in the thoracic aorta with PC-MRI-based boundary conditions: A least-square three-element Windkessel approach. Int J Numer Method Biomed Eng. 2018; 34: e3134.

22. Alli O, Jacobs L, Amanullah AM. Acute aortic syndromes: pathophysiology and management. Rev Cardiovasc Med. 2008; 9: 111-124.

23. Kharche SR, Stary T, Colman MA, Biktasheva IV, Workman AJ, Rankin AC, et al. Effects of human atrial ionic remodelling by β-blocker therapy on mechanisms of atrial fibrillation: a computer simulation. Europace. 2014; 16: 1524-1533.

24. Martinez-Pinna J, Marroqui L, Hmadcha A, Lopez-Beas J, Soriano S, Villar-Pazos S, et al. Oestrogen receptor β mediates the actions of bisphenol-A on ion channel expression in mouse pancreatic beta cells. Diabetologia. 2019; 62: 1667-1680.

25. Babiloni-Chust I, Dos Santos RS, Medina-Gali RM, Perez-Serna AA, Encinar JA, Martinez-Pinna J, et al. G protein-coupled estrogen receptor activation by bisphenol-A disrupts the protection from apoptosis conferred by the estrogen receptors ERα and ERβ in pancreatic beta cells. Environ Int. 2022; 164: 107250.

26. Braverman AC. Medical management of thoracic aortic aneurysm disease. J Thorac Cardiovasc Surg. 2013; 145: S2-S6.

27. Milewicz DM, Ramirez F. Therapies for Thoracic Aortic Aneurysms and Acute Aortic Dissections. Arterioscler Thromb Vasc Biol. 2019; 39: 126-136.

28. Siordia JA. Beta-Blockers and Abdominal Aortic Aneurysm Growth: A Systematic Review and Meta-Analysis. Curr Cardiol Rev. 2021; 17: e230421187502.

29. Kazuno K, Kinoshita H, Hori M, Yosizaki T, Tamura A, Sato H, et al. Endovascular treatment for mycotic aneurysm using pyoktanin-applied devices. CVIR Endovasc. 2020; 3: 55.

30. Bavaria JE, Appoo JJ, Makaroun MS, Verter J, Yu ZF, Mitchell RS, et al. Endovascular stent grafting versus open surgical repair of descending thoracic aortic aneurysms in low-risk patients: a multicenter comparative trial. J Thorac Cardiovasc Surg. 2007; 133: 369-377.

31. Desai ND, Burtch K, Moser W, Moeller P, Szeto WY, Pochettino A, et al. Long-term comparison of thoracic endovascular aortic repair (TEVAR) to open surgery for the treatment of thoracic aortic aneurysms. J Thorac Cardiovasc Surg. 2012; 144: 604-609.

32. Gopaldas RR, Huh J, Dao TK, LeMaire SA, Chu D, Bakaeen FG, et al. Superior nationwide outcomes of endovascular versus open repair for isolated descending thoracic aortic aneurysm in 11,669 patients. J Thorac Cardiovasc Surg. 2010; 140: 1001-1010.

33. Yoshida K, Nakamura K, Ishigami M, Kinoshita M, Koyama T. Staged graft replacement with thoracic endovascular aneurysm repair for an extensive thoracoabdominal aortic aneurysm after total arch replacement. J Cardiothorac Surg. 2022; 17: 20.

34. Scala M, Fiaschi P, Cama A, Consales A, Piatelli G, Giannelli F, et al. Radiation-Induced Moyamoya Syndrome in Children with Brain Tumors: Case Series and Literature Review. World Neurosurg. 2020; 135: 118-129.

35. Cecchi E, Giglioli C, Valente S, Lazzeri C, Gensini GF, Abbate R, et al. Role of hemodynamic shear stress in cardiovascular disease. Atherosclerosis. 2011; 214: 249-256.

36. Alimohammadi M. Aortic Dissection: Simulation Tools for Disease Management and Understanding. Cham: Springer International Publishing. 2018.

37. Chen SW, Lin YS, Wu VC, Lin MS, Chou AH, Chu PH, et al. Effect of β-blocker therapy on late outcomes after surgical repair of type A aortic dissection. J Thorac Cardiovasc Surg. 2020; 159: 1694-1703.e3.

38. Gijsen FJ, van de Vosse FN, Janssen JD. The influence of the non-Newtonian properties of blood on the flow in large arteries: steady flow in a carotid bifurcation model. J Biomech. 1999; 32: 601-608.

39. Ventre J, Politi MT, Fernández JM, Ghigo AR, Gaudric J, Wray SA, et al. Parameter estimation to study the immediate impact of aortic cross-clamping using reduced order models. Int J Numer Method Biomed Eng. 2021; 37: e3261.

40. Shi Y, Lawford P, Hose R. Review of zero-D and 1-D models of blood flow in the cardiovascular system. Biomed Eng Online. 2011; 10: 33.

41. Stone WM, Abbas M, Cherry KJ, Fowl RJ, Gloviczki P. Superior mesenteric artery aneurysms: is presence an indication for intervention? J Vasc Surg. 2002; 36: 234-237.

42. Williams B, Lacy PS; CAFE and the ASCOT (Anglo-Scandinavian Cardiac Outcomes Trial) Investigators. Impact of heart rate on central aortic pressures and hemodynamics: analysis from the CAFE (Conduit Artery Function Evaluation) study: CAFE-Heart Rate. J Am Coll Cardiol. 2009; 54: 705-713.

43. Tsukiyama H, Otsuka K, Higuma K. Effects of beta-adrenoceptor antagonists on central haemodynamics in essential hypertension. Br J Clin Pharmacol. 1982; 13: 269S-278S.

44. Heijmen RH, Deblier IG, Moll FL, Dossche KM, van den Berg JC, Overtoom TT, et al. Endovascular stent-grafting for descending thoracic aortic aneurysms. Eur J Cardiothorac Surg. 2002; 21: 5-9.

45. Chiesa R, Tshomba Y, Civilini E, Marone EM, Bertoglio L, Baccellieri D, et al. Open repair of descending thoracic aneurysms. HSR Proc Intensive Care Cardiovasc Anesth. 2010; 2: 177-190.

46. LeMaire SA, Price MD, Green SY, Zarda S, Coselli JS. Results of open thoracoabdominal aortic aneurysm repair. Ann Cardiothorac Surg. 2012; 1: 286-292.

47. Coselli JS. Reflection of pioneers: redo thoracoabdominal aortic aneurysm repair controversies in thoracic aortic aneurysm surgery. Gen Thorac Cardiovasc Surg. 2019; 67: 168-174.

48. Selle JG, Robicsek F, Daugherty HK, Cook JW. Thoracoabdominal aortic aneurysms. A review and current status. Ann Surg. 1979; 189: 158-164.

49. Armour CH, Guo B, Pirola S, Saitta S, Liu Y, Dong Z, et al. The influence of inlet velocity profile on predicted flow in type B aortic dissection. Biomechanics and Modeling in Mechanobiology. 2021; 20: 481-490.

50. Gawenda M, Aleksic M, Heckenkamp J, Reichert V, Gossmann A, Brunkwall J. Hybrid-procedures for the treatment of thoracoabdominal aortic aneurysms and dissections. Eur J Vasc Endovasc Surg. 2007; 33: 71-77.

51. Genoni M, Paul M, Jenni R, Graves K, Seifert B, Turina M. Chronic beta-blocker therapy improves outcome and reduces treatment costs in chronic type B aortic dissection. Eur J Cardiothorac Surg. 2001; 19: 606-610.

52. Erbel R, Aboyans V, Boileau C, Bossone E, Bartolomeo RD, Eggebrecht H, et al. 2014 ESC Guidelines on the diagnosis and treatment of aortic diseases: Document covering acute and chronic aortic diseases of the thoracic and abdominal aorta of the adult. The Task Force for the Diagnosis and Treatment of Aortic Diseases of the European Society of Cardiology (ESC). Eur Heart J. 2014; 35: 2873-2926.

53. Fox N, Schwartz D, Salazar JH, Haut ER, Dahm P, Black JH, et al. Evaluation and management of blunt traumatic aortic injury: a practice management guideline from the Eastern Association for the Surgery of Trauma. J Trauma Acute Care Surg. 2015; 78: 136-146.

54. Kanematsu Y, Kanematsu M, Kurihara C, Tsou TL, Nuki Y, Liang EI, et al. Pharmacologically induced thoracic and abdominal aortic aneurysms in mice. Hypertension. 2010; 55: 1267-1274.

55. Laurent S, Cockcroft J, Van Bortel L, Boutouyrie P, Giannattasio C, Hayoz D, et al. European Network for Non-invasive Investigation of Large Arteries. Expert consensus document on arterial stiffness: methodological issues and clinical applications. Eur Heart J. 2006; 27: 2588-2605.

56. Mitchell GF, Jen Hwang S, Vasan RS, Larson MG, Pencina MJ, Hamburg NM, et al., Arterial Stiffness and Cardiovascular Events. Circulation, 2010; 121: 505-511.

57. De Paulis S, Arlotta G, Calabrese M, Corsi F, Taccheri T, Antoniucci ME, et al. Postoperative Intensive Care Management of Aortic Repair. J Pers Med. 2022; 12: 1351.

58. Denault AY, Chaput M, Couture P, Hébert Y, Haddad F, Tardif JC. Dynamic right ventricular outflow tract obstruction in cardiac surgery. J Thorac Cardiovasc Surg. 2006; 132: 43-49.

59. Filipovic N, Milasinovic D, Zdravkovic N, Böckler D, von Tengg-Kobligk H. Impact of aortic repair based on flow field computer simulation within the thoracic aorta. Comput Methods Programs Biomed. 2011; 101: 243-252.

60. Tigkiropoulos K, Sigala F, Tsilimigras DI, Moris D, Filis K, Melas N, et al. Endovascular Repair of Blunt Thoracic Aortic Trauma: Is Postimplant Hypertension an Incidental Finding? Ann Vasc Surg. 2018; 50: 160-166.e1.

61. Griepp RB, Stinson EB, Hollingsworth JF, Buehler D. Prosthetic replacement of the aortic arch. J Thorac Cardiovasc Surg. 1975; 70: 1051-1063.

62. Mohammed RK, Cheung S, Parikh SP, Asgaria K. Conservative management of aortic arch injury following penetrating trauma. Ann R Coll Surg Engl. 2015; 97: 184-187.

63. von Spiczak J, Crelier G, Giese D, Kozerke S, Maintz D, Bunck AC. Quantitative Analysis of Vortical Blood Flow in the Thoracic Aorta Using 4D Phase Contrast MRI. PLoS One. 2015; 10: e0139025.

64. Prahl Wittberg L, van Wyk S, Fuchs L, Gutmark E, Backeljauw P, Gutmark-Little I. Effects of aortic irregularities on blood flow. Biomech Model Mechanobiol. 2016; 15: 345-360.

65. Akuzawa N, Kurabayashi M, Suzuki T, Yoshinari D, Kobayashi M, Tanahashi Y, et al. Spontaneous isolated dissection of the superior mesenteric artery and aneurysm formation resulting from segmental arterial mediolysis: a case report. Diagn Pathol. 2017; 12: 74.

66. Chatzizisis YS, Coskun AU, Jonas M, Edelman ER, Feldman CL, Stone PH. Role of endothelial shear stress in the natural history of coronary atherosclerosis and vascular remodeling: molecular, cellular, and vascular behavior. J Am Coll Cardiol. 2007; 49: 2379-2393.

67. Chiu JJ, Chien S. Effects of disturbed flow on vascular endothelium: pathophysiological basis and clinical perspectives. Physiol Rev. 2011; 91: 327-387.

68. Jackson ZS, Gotlieb AI, Langille BL. Wall tissue remodeling regulates longitudinal tension in arteries. Circ Res. 2002; 90: 918-925.

69. Frauenfelder T, Lotfey M, Boehm T, Wildermuth S. Computational fluid dynamics: hemodynamic changes in abdominal aortic aneurysm after stent-graft implantation. Cardiovasc Intervent Radiol. 2006; 29: 613-623.

70. Deplano V, Knapp Y, Bertrand E, Gaillard E. Flow behaviour in an asymmetric compliant experimental model for abdominal aortic aneurysm. J Biomech. 2007; 40: 2406-2413.

71. Davies PF. Hemodynamic shear stress and the endothelium in cardiovascular pathophysiology. Nat Clin Pract Cardiovasc Med. 2009; 6: 16-26.

72. Soaers AF. Carvalho, Leite A. Wall Shear Stress-Based Hemodynamic Descriptors in the Abdominal Aorta Bifurcation: Analysis of a Case Study. J ApplFluid Mechanics. 2021; 14.

73. Peng C, Liu J, He W, Qin W, Yuan T, Kan Y, et al. Numerical simulation in the abdominal aorta and the visceral arteries with or without stenosis based on 2D PCMRI. Int J Numer Method Biomed Eng. 2022; 38: e3569.

74. Liu X, Pu F, Fan Y, Deng X, Li D, Li S. A numerical study on the flow of blood and the transport of LDL in the human aorta: the physiological significance of the helical flow in the aortic arch. Am J Physiol Heart Circ Physiol. 2009; 297: H163-170.

75. Trenti C, Ziegler M, Bjarnegård N, Ebbers T, Lindenberger M, Dyverfeldt P. Wall shear stress and relative residence time as potential risk factors for abdominal aortic aneurysms in males: a 4D flow cardiovascular magnetic resonance case-control study. J Cardiovasc Magn Reson. 2022; 24: 18.

76. Alimohammadi M, Pichardo-Almarza C, Agu O, Díaz-Zuccarini V. Development of a Patient-Specific Multi-Scale Model to Understand Atherosclerosis and Calcification Locations: Comparison with In vivo Data in an Aortic Dissection. Front Physiol. 2016; 7: 238.